Mendes, Marcelo; Favoreto, Julia; Nunes, Marcos; Rigueti, Ariely; Valle, Bruno; Borghi, Leonardo; Corbett, Patrick; Lima, Maira; Martins, Lorena; Arena, Michele

Petrophysical Characterization and Porosity-Permeability Log Calculation by Dual-Energy CT Scan: Morro do Chaves Formation, Sergipe-Alagoas Basin, Brazil

Petrophysical Characterization and Porosity-Permeability Log Calculation by Dual-Energy CT Scan: Morro do Chaves Formation, Sergipe-Alagoas Basin, Brazil

Caracterização Petrofísica e Cálculo de Perfis de Porosidade-Permeabilidade por Tomografia Computadorizada de Dupla Energia: Formação Morro do Chaves, Bacia de Sergipe-Alagoas, Brasil

Marcelo Mendes[1] , Julia Favoreto[1] , Marcos Nunes[1] , Ariely Rigueti[1] , Bruno Valle[1] ,
Leonardo Borghi[1] , Patrick Corbett[2] , Maira Lima[1] , Lorena Martins[1] , Michele Arena[1]

[1] Universidade Federal do Rio de Janeiro, Instituto de Geociências, Departamento de Geologia, Rio de Janeiro, RJ, Brasil
[2] Heriot-Watt University, Institute of Petroleum Engineering, Edinburgh, United Kingdom

E-mails: marcelomendes79@hotmail.com; julia@geologia.ufrj.br; mnunesgo@gmail.com; luparellirigueti@gmail.com; bruno@geologia.ufrj.br; lborghi@geologia.ufrj.br; p.w.m.corbett@hw.ac.uk; mairalimarj@gmail.com; lorenapmartins8@gmail.com; michele@geologia.ufrj.br
Corresponding author: Marcelo Mendes; marcelomendes79@hotmail.com

Abstract

Considered important analogues of pre-salt reservoirs in hydrocarbon-producing basins throughout eastern Brazilian shore, the coquinas of the Morro do Chaves Formation (Barremian-Aptian of the Sergipe-Alagoas Basin) were studied in this work from a petrophysical standpoint using advanced characterization methods for cores recovered from four wells (2-SMC-01-AL, 2-SMC-02-AL, 2-SMC-03-AL e 2-SMC-01-AL) drilled in the Atoll Quarry, which is located in city of São Miguel dos Campos, Alagoas State, Brazil. To understand the relationships between lithological and diagenetic heterogeneities that control the distribution of permeability-porosity properties of this Rock Type, the cores underwent Dual-Energy X-ray imaging, which determines bulk density and photoelectric factor data to define seven Rock Types and generate effective porosity curves for the studied wells. Permeabilities in the wells were modeled based on the Flow Zone Index (FZI) concept, and each reservoir interval based on the Global Hydraulic Elements (GHEs) approach. Results were calibrated with laboratory measurements in plugs, and porosity was classified by petrographic analysis by Digital Image Analysis (DIA). All wells were correlated and four internal flooding surfaces identified, with a regressive surface (RS) dividing the Morro do Chaves Formation into an upper section with better reservoir characteristics and a lower one with worse ones.

Keywords: Rock types; Tomography; Coquina

Resumo

Consideradas importantes análogos aos reservatórios do Pré-sal das bacias produtoras de hidrocarbonetos da margem leste brasileira, as coquinas da Formação Morro do Chaves (Barremiano-Aptiano da Bacia de Sergipe-Alagoas) foram estudadas neste trabalho sob o ponto de vista petrofísico através de métodos avançados de caracterização dos testemunhos recuperados de quatro poços (2-SMC-01-AL, 2-SMC-02-AL, 2-SMC-03-AL e 2-SMC-01-AL) perfurados na Pedreira Atol no município de São Miguel dos Campos-AL. Com o objetivo de se compreender as relações entre as heterogeneidades litológicas e diagenéticas que atuam no controle da distribuição das características permo-porosas desse tipo de rocha, os testemunhos foram submetidos ao imageamento de Raio-X com dupla energia que forneceram dados de densidade e fator fotelétrico para a definição de sete *Rock Types* e para a modelagem da curva de porosidade efetiva dos poços estudados. As permeabilidades dos poços foram modeladas com base no conceito de *Flow Zone Index* (FZI) e cada intervalo do reservatório foi classificado baseado no conceito de *Global Hydraulic Elements* (GHE). Os resultados foram calibrados através de medidas de laboratório em plugs e o tipo de porosidade classificada através de análises petrográficas com o auxílio do método de Análise Digital de Imagens (ADI). Todos os poços foram correlacionados e quatro superfícies internas foram identificadas, sendo a superfície regressiva (RS) a que divide a Formação Morro do Chaves em seção superior, com melhores características de reservatório, e a seção inferior, com piores características de reservatório.

Palavras-chave: Rock types; Tomografia; Coquina

1 Introduction

The growing economic interest in recent oil discoveries in the Pre-salt interval of the Santos Basin (e.g., coquinas and microbialites) has required knowledge about genesis and faciological and diagenetic heterogeneities that control petrophysical distribution, which are characteristic of such carbonate rocks. Due to the large thicknesses and oil accumulations in coquinas, these reservoirs have been the subject of sedimentological, taphonomic, and petrophysical studies (Chinellato, Vidal & Kuroda 2018; Thompson, Stilwell & Hall 2015). In this context, the coquinas of the Morro do Chaves Formation (Barremian-Aptian of the Sergipe-Alagoas Basin) has featured in studies of reservoirs analogous to the pre-salt interval in hydrocarbon-producing basins throughout eastern Brazilian shore (Kinoshita 2010). In the studied area, the Morro do Chaves Formation is around 200 m thick (Rigueti et al. 2020) and characterized by interlayers of coquinas, sandstones, and shales. These, in turn, characterize a mixed depositional paleoenvironment, where typical carbonate and siliciclastic depositional processes occur in a dynamic environment (Azambuja, Arienti & Cruz 1998; Favoreto et al. 2021; Rigueti et al. 2020; Tavares et al. 2015). However, lithofaciological analysis alone does not reflect all potential conditions in this reservoir in the Morro do Chaves Formation, besides being insufficient to define permeability-porosity characteristics within this interval, mainly where rocks were strongly influenced by diagenesis. As in most carbonate reservoirs, the main challenge is to determine the pore space distribution in coquinas, which is usually complex and difficult to predict, as well as their permeability (Câmara 2013; Corbett et al. 2016 and Corbett et al. 2017). As an alternative to porosity and permeability estimation methods and their characterization, this paper presents an advanced core characterization methodology for coquinas, integrating X-rays, Dual-energy CT scan, as well as geological and conventional core analyses to fully understand the reservoir.

2 Geological Settings

The Sergipe-Alagoas Basin is a vast elongated depression (40,000 km²) located in northeastern Brazil, oriented in the NE direction and bounded on the north by the Alto Maragogi and on the south by the Vaza-Barris fault system (Azambuja, Arienti & Cruz 1998). This basin was formed in the context of the Afro-Brazilian Depression during the Early Cretaceous. Its sedimentary fill shows several tectonic phases related to the rupture of the Gondwana supercontinent, culminating in the formation of the South Atlantic Ocean (Cainelli & Mohriak 1999). This process can be divided into five supersequences (Campos Neto, Souza-Lima & Cruz 2007), namely: sag phase (Permian-Carboniferous), pre-rift (Late Jurassic-Early Cretaceous), rift (Early Cretaceous – Barresian to Aptian), post-rift (Early Cretaceous – Aptian to Albian) and drift stage (Mesozoic-Cenozoic). The Morro do Chaves Formation is related to the rift phase of the Sergipe-Alagoas Basin and was formed at the end of the Barremian and beginning of the Aptian. Its sedimentary column may exceed 300 m in thickness (Azambuja, Arienti & Cruz 1998) and is composed of coquinas interbedded with sandstones and shales deposited in a lacustrine environment, with depositional cycles controlled by climate and tectonics (Rigueti et al. 2020). Thus, the Morro do Chaves Formation represents a third-order transgressive system tract in the Sergipe-Alagoas Basin. The bivalve and fish species identified therein were associated with water salinity, suggesting a marine connection in the sedimentary paleoenvironment (Azambuja, Arienti & Cruz 1998; Figueiredo 1981; Thompson, Stilwell & Hall 2015).

3 Methodology and Data

This study was carried out using dual-energy X-ray tomography images obtained over 562.2 meters of well cores, as well as 142 core plugs, 221 petrographic thin-sections, and Gamma Ray log and caliper log runs from four wells drilled around the Atoll Quarry (Table 1).

This quarry is known for having a large exposure interval of the Morro do Chaves Formation due to mining by the InterCement company, in the city of São Miguel dos Campos, AL - Brazil (Figure 1). The wells were drilled and cored using the MACH-1200 drilling rig supplied by the Geology Department of the Federal University of Rio de Janeiro. The rig recovered 63 mm diameter cores from cylindrical rock samples, which were described at a 1:40

Table 1 Summary of the material used in this study.

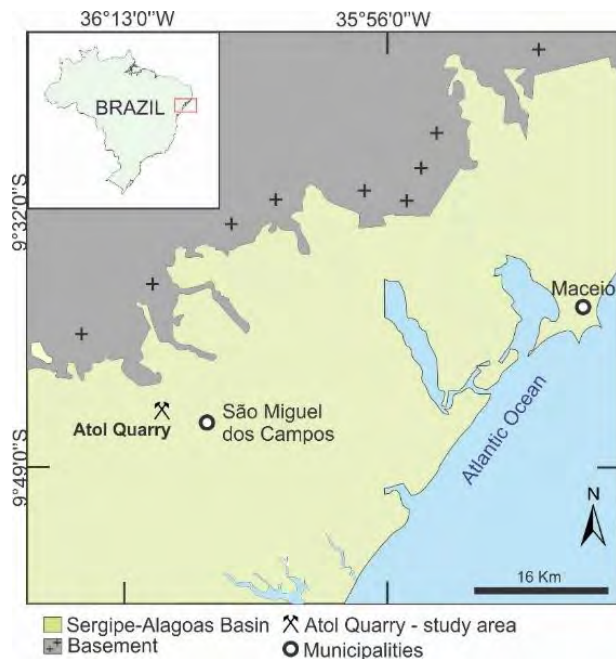| Well	Coordinates		Length (m)	Number of Plugs	Number of thin-sections
2-SMC-01-AL	9°45'37,75"S	36°10'88"00"O	134,6	50	70
2-SMC-02-AL	9°45'29,05"S	36°09'10,65"O	183,6	46	80
2-SMC-03-AL	9°45'07,59"S	36°09'17,54"O	159,5	31	44
2-SMC-04-AL	9°45'28,10"S	36°09'21,70"O	84,5	15	27

Figure 1 Location map of the Atoll quarry near the city of São Miguel dos Campos – AL (Brazil). The Sergipe-Alagoas Basin and crystalline basement**.**

scale, as proposed by Dal'Bó et al. (2021). The cores were thereafter submitted to dual-energy X-ray tomography imaging by the company INGRAIN. This technique acquires images at two different energy levels (90KeV and 120KeV). The high level is more sensitive to rock bulk density (RHOB), while the low one is to rock mineralogy (Al-Owihan et al. 2014).

Bulk density (RHOB) and effective atomic number (Zeff) were independently calculated for each tomography slice along the cores every 0,5 millimeters (Wellington & Vinegar 1987). The Zeff parameter is related to the Photoelectric Factor (PEF), which is commonly used in oil well logging. The RHOB and PEF well log data were graphically combined to distinguish each Rock Type (RT) group per well. The cut-off values for the definition of Rock-Types were established according to the concentration of points identified in the RHOB x PEF chart for each well and further refined based on lithological criteria. One-inch diameter core plugs were obtained from the cores according to faciological and visual porosity criteria. The plug samples were used in petrophysical laboratory tests following the procedure API RP 40 standard to perform the Routine Core Analysis (RCAL), under outcrop confinement pressure (500 psi). Afterwards, thin-sections were obtained from core plugs regions and scanned under a Zeiss Imager A2m microscope to classify porosity through digital image analysis (DIA) (Weger 2006). The Gamma Ray log, which

detects natural radioactivity from unstable elements (^{238}U, ^{232}Th, and ^{40}K) in lithologies, was used for rock-well log and between-well correlations and clay volume (VSH) log estimation within the core interval. The VSH logs were combined with total porosity logs to calculate effective porosity log, and the result was compared with porosity plug measurements to verify correspondence between the obtained values. Flow Zone Index (FZI) was defined to obtain permeability equations and generate permeability logs for each well.

4 Results and Discussions

4.1 Rock Types

The RHOB and PEF log data from Dual-energy CT scan provided extensive information, which was used to integrate routine core analysis (RCAL) data and core descriptions. Seven Rock Types (RT-1 to RT-7) were defined according the cut-off values in the RHOB and PEF cross plot for each well and characterized according to a set of lithological and petrophysical aspects (Figure 2). Rock Type 1 (RT-1) was represented by the Muddy Dispersestone (Md) lithology (Dal'Bó et al. 2021), which was composed of more than 85% matrix (clay and silt) and less than 15% bioclasts, regardless of size and fragmentation degree, and with dispersed concentrations of articulated shells. Rock Type 2 (RT-2) was represented by the Sandy Dispersestone (Sd) lithology, which was composed of 90% or more of siliciclastic fine grains and less than 10% of bioclast fragments, regardless of size or shell fragmentation degree (Favoreto et al. 2021). RT-2 was also represented by the Sandy Loosestone (sL) lithology, which was composed of 50 to 85% of fine siliciclastic sand grains and 15 to 50% of disarticulated shells. Rock Type 3 (RT-3) was represented by the Sorted Shellstone (sS) lithology, which was composed of 75 to 90% of bioclast fragments and 25 to 10% of sand-sized siliciclastic components (Dal'Bó et al. 2021). RT-3 was also represented by the Shellstone (S), which was composed of 75 to 90% of bioclast fragments and 25 to 10% of matrix, and by the Sandy Densestone (sD) lithology, which was composed of about 25% of silt- and sand-sized siliciclastic material and 75% of bioclast fragments. Rock Type 4 (RT-4) was represented by the Shellstone (S), which was mostly composed of more than 90% of bioclast fragments and less than 10% of matrix. Higher shell proportions compared to those of matrix contents stems from the winnowing process, by which fine grains were removed from the matrix. RT-4 was also represented by the Sorted Shellstone (sS) but with a greater
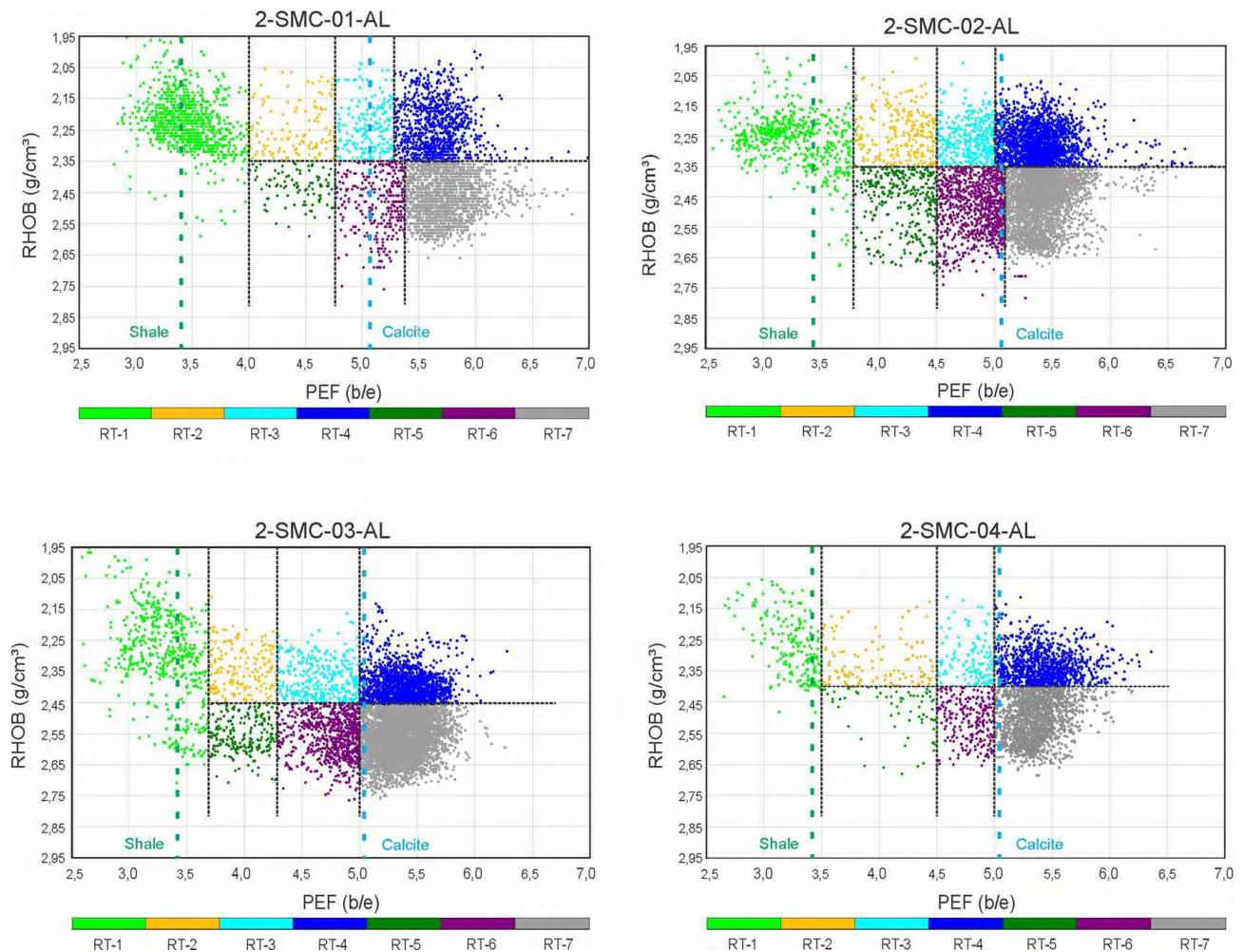
Figure 2 Rock Types cut-offs to define each RT.

proportion than that of RT-3, and composed of more than 90% of bioclast fragments and less than 10% of sand-sized siliciclastic components.

Further, RT-4 was also represented by the Rounded Shellstone (rS), which has more than 90% reworked bioclast fragments and less than 10% sand-sized siliciclastic components. The bioclasts in this Rock Type were well selected, disarticulated, and fragmented, because of a strong dynamic deposition environment (Dal'Bó et al. 2021). Rock Type 5 (RT-5) was represented by the Muddy Densestone (mD), which was composed of 25% of fine grains (clay and silt) and 75% of bioclast fragments, regardless of size or fragmentation degree. Condensed Shellstones (cS) were present in less proportion and were composed of 75% of bioclasts, with dissolution seams increasing clay concentrations due to insoluble material (Dal'Bó et al. 2021). Rock Type 6 (RT-6) was represented by the Condensed Shellstone (cS), which was composed of more than 80% bioclasts, as well as cemented and

sutured contact surfaces (Dal'Bó et al. 2021). RT-6 was also represented by the Sandy Densestone (sD), which was composed of 25% of silt- and sand-sized siliciclastic material and 75% of bioclast fragments with compression effect. Rock Type 7 (RT-7) was represented by the Sparstone (Sp), where primary features were obliterated and replaced with diagenetic textures. RT-7 was also represented by the Fitted Shellstone (fS), which was composed of more than 90% of bioclasts, with framework supported by shells with sutured contact surfaces and stylolites. All Rock Types and their petrophysical parameters are summarized in Table 2.

Rock Types composed of highly clayey lithologies had lower average porosity than those with lower matrix and cement contents than bioclasts, especially highly fragmented ones. When associated with dissolution events, diagenesis enhances permeability-porosity properties in rocks, but can also markedly reduce porosity if associated with compaction and cementation events (Corbett et al. 2017; Lima et al. 2019; Nunes et al. 2021).

4.2 Porosity Characterization

Six porosity types were identified in the four wells drilled in the Atoll quarry, three selective and three nonselective porosity types (Choquette & Pray 1970). In selective porosity (Figure 3), particle or crystal arrangements were directly related to depositional events, and the pore boundaries do not overlap with constituent boundaries, namely: interparticle, intercrystalline, and moldic types. In nonselective porosity (Figure 4), the porous system had no direct relationship with the arrangement of rock constituents, and pore boundaries overlap with

constituent boundaries, besides being directly related to diagenetic processes, namely: vug, stylolite with dissolution, and fracture types.

Interparticle type is a selective porosity of depositional origin (primary) existing between siliciclastic grains and shell fragments. These can be featured by preferential dissolution of matrix components or cement, thus increasing pore size (Choquette & Pray 1970). In the Morro do Chaves Formation coquinas, interparticle porosity can reach average values of 12%. In such cases, porous space architecture can present high connectivity and provide an average permeability of 170 mD. Table 3 summarizes

Table 2 Summary table of the parameters of Rock Types composing coquina (Dal´Bó et al. 2021).

Lithology	Main porosity type	Average porosity	Average Permeability
RT-2	Interparticle and moldic	15%	52 mD
RT-3	Interparticle and moldic	16%	303 mD
RT-4	Moldic, interparticle and vug	17%	370 mD
RT-5	Moldic and interparticle	10%	2 mD
RT-6	Interparticle, moldic and stylolites	12%	15 mD
RT-7	Moldic, fractures, vug and intercrystalline	11%	30 mD

Figure 3 A. thin-section showing the interparticle porosity type and laboratory measurement; A'. 2D binary image showing the interparticle porosity type and ADI result; B. thin-section showing the moldic porosity type and laboratory measurement; B'. 2D binary image showing the moldic porosity type and ADI result; C. thin-section showing the intercrystalline porosity type and laboratory measurement; C'. 2D binary image showing the intercrystalline porosity type and ADI result.

Figure 4 A. thin-section showing the vug porosity type and laboratory measurement; A'. 2D binary image showing the vug porosity type and ADI result; B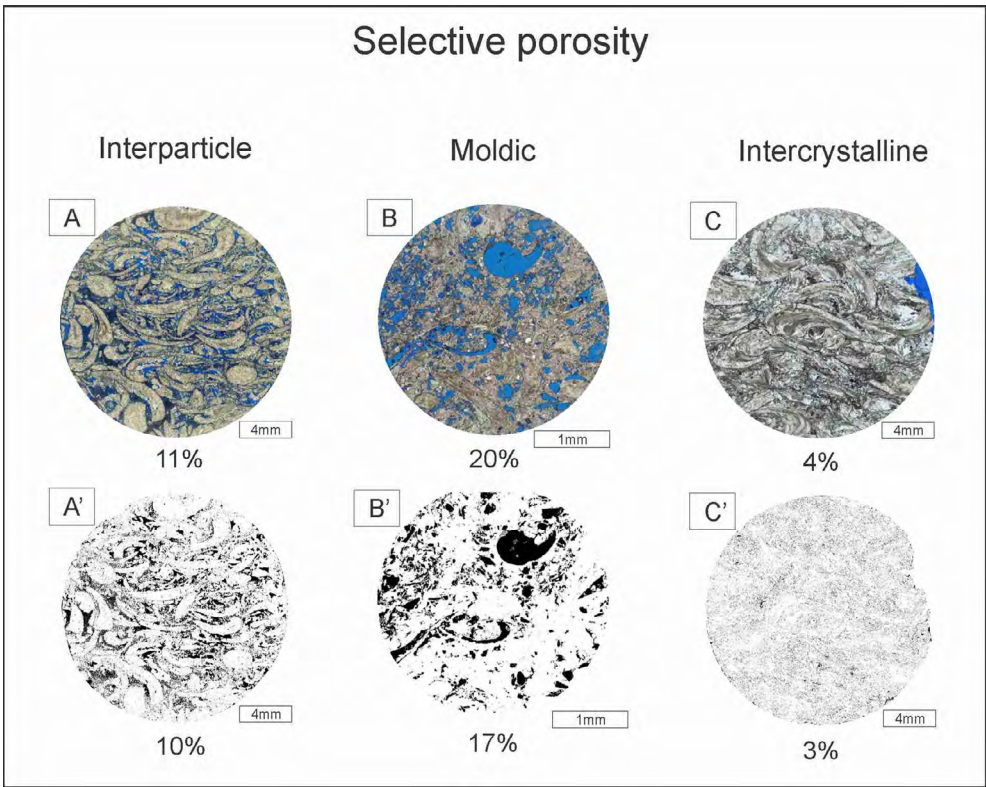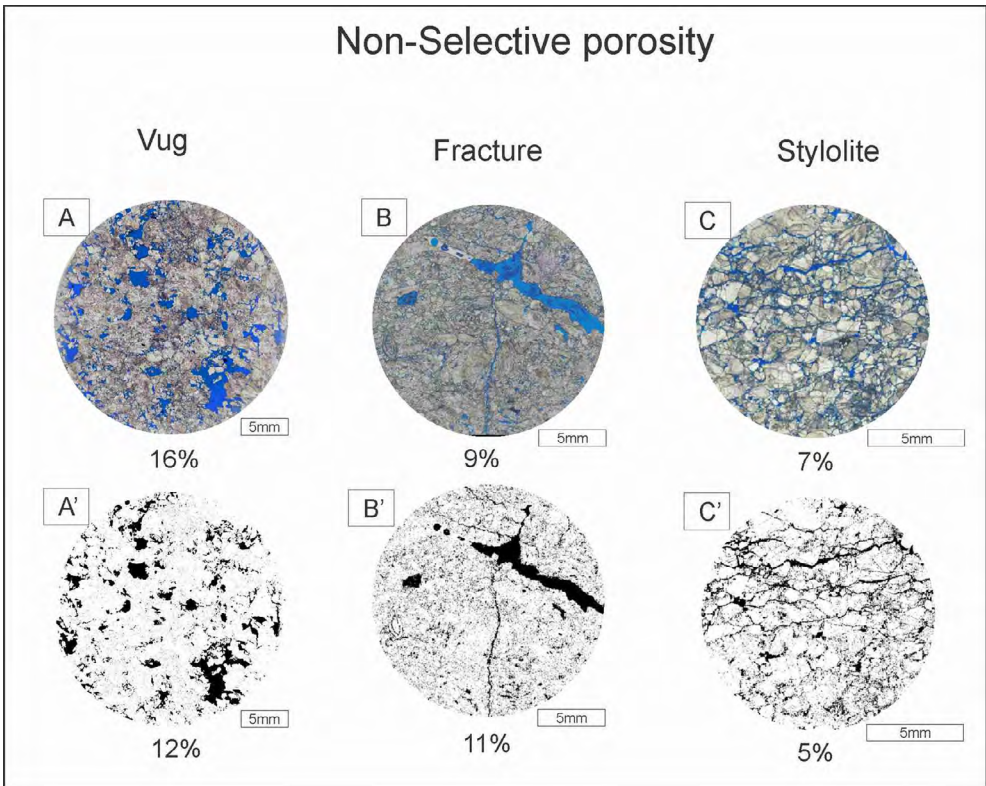. thin-section showing the fracture porosity type and laboratory measurement; B'. 2D binary image showing the fracture porosity type and ADI result; C. thin-section showing the stylolite porosity type and laboratory measurement; C'. 2D binary image showing the stylolite porosity type and ADI result.

Table 3 Summary of the average porosity and permeability for each porosity type.

Porosity type	Average porosity	Average permeability
Interparticle	12%	170 mD
Moldic	15%	156 mD
Intercrystalline	7%	2 mD
Vug	16%	752 mD
Fracture	10%	591 mD
Stylolite	4%	-

the porosity types and their averages obtained by laboratory measurements on core plugs, as well as the corresponding permeability averages. These data show that the highest porosity and permeability averages were related to vug porosity. Although moldic porosity has the second highest average for the studied wells, it was lower than fracture and interparticle types. Still, 156 mD can be considered high for such porosity type. One explanation may be related to the evolution of bioclast dissolution, connecting moldic pores and increasing average permeability of samples with this porosity type. Câmara (2013) classified moldic porosity as connected when a set of moldic pores has more than 10% of

connectivity. Fracture type has the fourth highest average porosity and second highest average permeability, measured in plugs with integrity to perform the laboratory tests.

Stylolite porosity has the lowest average porosity and permeability, since this type occurs in association with high compaction and cementation lithologies. The thin-sections used for porosity type identification were also applied in porosity calculation by the Digital Image Analysis (DIA) method, with the results being then compared with laboratory data in plugs. These methods showed porosity differences of up to 15%. These differences may be related to DIA spatial dimension since such measurement on

thin-sections was performed in two-dimensions (2D), while laboratory measurements on plugs were in three-dimensions (3D). Therefore, the evaluation of pore geometric properties becomes limited in terms of the three-dimensional physical property of the samples. Accordingly, thin-section porosity estimates by DIA were used qualitatively in this study.

Nonselective porosities identified in the Morro do Chaves Formation were generally associated with lithological intervals with higher cementation degrees or more intense recrystallization of the entire rock framework. Thus, average porosities were reduced, and DIA analysis was even more limited.

4.3 Effective Porosity Log Calculation

Effective porosity logs (Φe_D) were calculated for the studied wells using Dual-energy CT scan RHOB logs on cores, which provide rock electrical density measures, which in turn were directly related to rock matrix density and inversely related to porosity. Initially, total porosity was calculated (Equation 1), and later combined with VSH log to estimate effective porosity (Equation 2). To this end, individual densities of the involved materials must

be previously known, as well as grain and interstitial fluid densities.

$$\Phi T = (\rho ma - \rho b) / (\rho ma - \rho f) \qquad \textbf{(1)}$$

Total porosity log (ΦT) was calculated as the ratio of matrix density differences (ρma), which was the average density obtained in the laboratory (2.71 g/cm³) for coquina rocks in the Morro do Chaves Formation, and the Formation volumetric density (ρb), which was measured by the RHOB log divided by the difference between the fluid density (ρf), which, in the case of Dual-energy CT scan, was the air (0.0012g/cm³ at 20°C - 1 atm) and matrix density (ρma). Effective porosity log (Φe) results from a combination between clay volume (Vsh) log and total porosity log (ΦT), as in Equation 2.

$$\Phi e = \Phi T * (1\text{-}Vsh) \qquad \textbf{(2)}$$

Effective porosity log results were compared with laboratory-measured core plug porosities for validation (Figure 5). Effective porosity refers to connected pores, so clay volume was taken from porosity log calculations and then compared with laboratory data, which measure
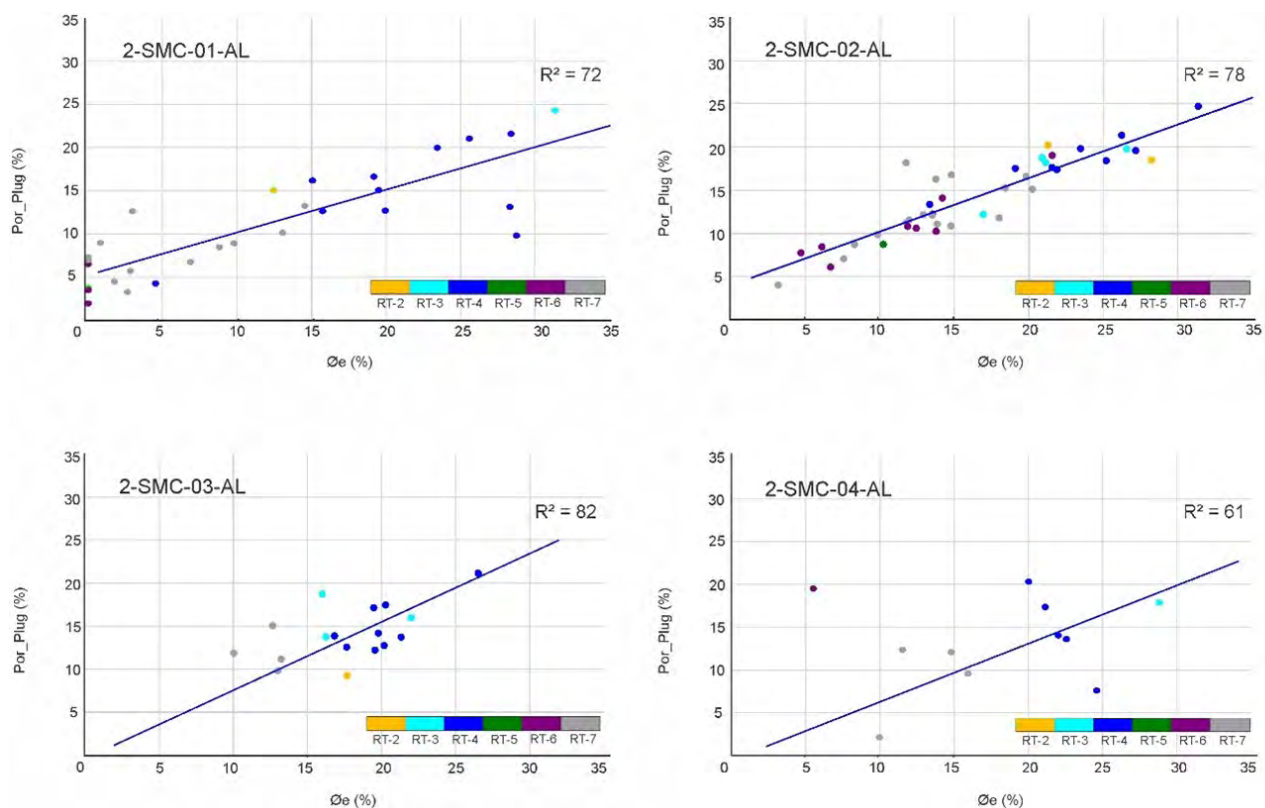

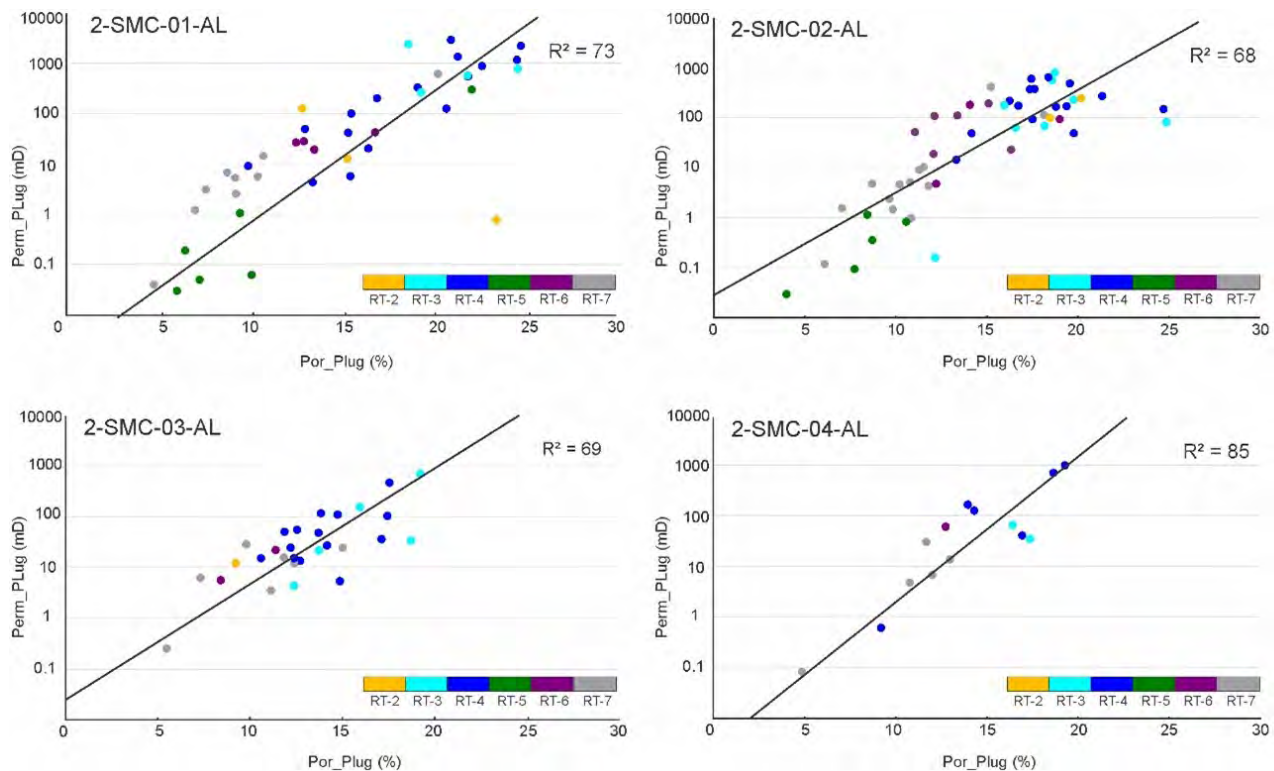**Figure 5** Rock Types in the *Φe vs.* Por_Plug cross-plot for each well.

Figure 6 Laboratory measurements of plugs for each well. Note that correlations were high for RT3 and RT4, moderate for RT-6, and low for RT-5 and RT-7.

connected porosity within the sample. Except for well 2-SMC-04-AL, which had a coefficient of determination (R^2) of 61%, all others had correlations with R^2 equal to or above 72%.

4.4 Permeability Log Calculation

The Permeability (K) was directly related to fluid mobility through porous media, which was directly related to rock porous connectivity. Since coquinas were highly heterogeneous, their effective porosity may include primary porosities and/or secondary porosities that, due to diagenetic evolution, may connect previously isolated pores. The permeability and porosity relationship was checked for each well studied by cross-plotting (Por_Plug vs. Perm_Plug) the laboratory data (Figure 6). The plot showed a direct relationship between porosity and permeability, with higher porosities representing connected pores, thus reflecting the high permeabilities of the sampled intervals. The Rock Types RT-3 and RT-4 had the highest porosity and permeability values since they were composed of coquinas from high-energy environments, with greater grain fragmentation and increased porosity due to dissolution events. The Rock Type RT-6, which composed of Densestone coquinas, had moderate porosity

and permeability, while RT-5 and RT-7 had lower ratio, porosity, and permeability for being composed of clay matrix and cemented/recrystallized coquinas, respectively.

Due to the high correspondence between porosity and permeability data, effective porosity logs were used as inputs to generate permeability logs by the Flow Zone Indicator (FZI) method. This approach incorporates not only petrophysical rock features, but also geological properties such as texture and mineralogy, which were directly related to distinct depositional events and diagenetic processes (Amaefule et al. 1993). Thus, through this, the different types of coquinas could be systematically compared (Corbett et al. 2017). Four FZI groups were manually defined as a function of the best fit between porosity and permeability data, providing the permeability functions in Table 4 and respective R^2 values.

To assess flow capacity at different reservoir intervals, laboratory porosity and permeability data were plotted on Global Hydraulic Unit - GHE graphs (Figure 7) to check for trends in the petrophysical properties of the Rock Types (Corbett & Potter 2004). Seven Global Hydraulic Elements (GHE-2, GHE-3, GHE-4, GHE-5, GHE-6, GHE-7, and GHE-8) were found, dividing the Rock Types into different hydraulic behaviors. GHE-2 and GHE-3 had a predominance of RT-5, which was composed

Table 4 Summary table of each FZI, permeability equation, and coefficients of determination (R^2) for each well.

| Well name	FZI	Equation	R^2
	FZI-1	$K = \Phi^{6,85} \times 10^{6,56}$	0,89
2-SMC-01-AL	FZI-2	$K = \Phi(4,75) \times 10^{5,33}$	0,97
	FZI-3	$K = \Phi(3,97) \times 10^{5,05}$	0,99
	FZI-4	$K = \Phi^{2,43} \times 10^{4,30}$	0,78
	FZI-1	$K = \Phi^{4,31} \times 10^{4,08}$	0,82
2-SMC-02-AL	FZI-2	$K = \Phi^{4,01} \times 10^{4,43}$	0,96
	FZI-3	$K = \Phi^{3,75} \times 10^{4,60}$	0,97
	FZI-4	$K = \Phi^{2,67} \times 10^{4,24}$	0,81
	FZI-1	$K = \Phi^{5,86} \times 10^{5,93}$	0,97
2-SMC-03-AL	FZI-2	$K = \Phi^{4,56} \times 10^{5,18}$	0,90
	FZI-3	$K = \Phi^{4,21} \times 10^{5,15}$	0,97
	FZI-4	$K = \Phi^{3,43} \times 10^{4,79}$	0,97
	FZI-1	$K = \Phi^{6,20} \times 10^{6,28}$	0,99
2-SMC-04-AL	FZI-2	$K = \Phi^{6,02} \times 10^{6,43}$	0,98
	FZI-3	$K = \Phi^{5,70} \times 10^{6,73}$	1,00
	FZI-4	$K = \Phi^{4,08} \times 10^{5,50}$	1,00
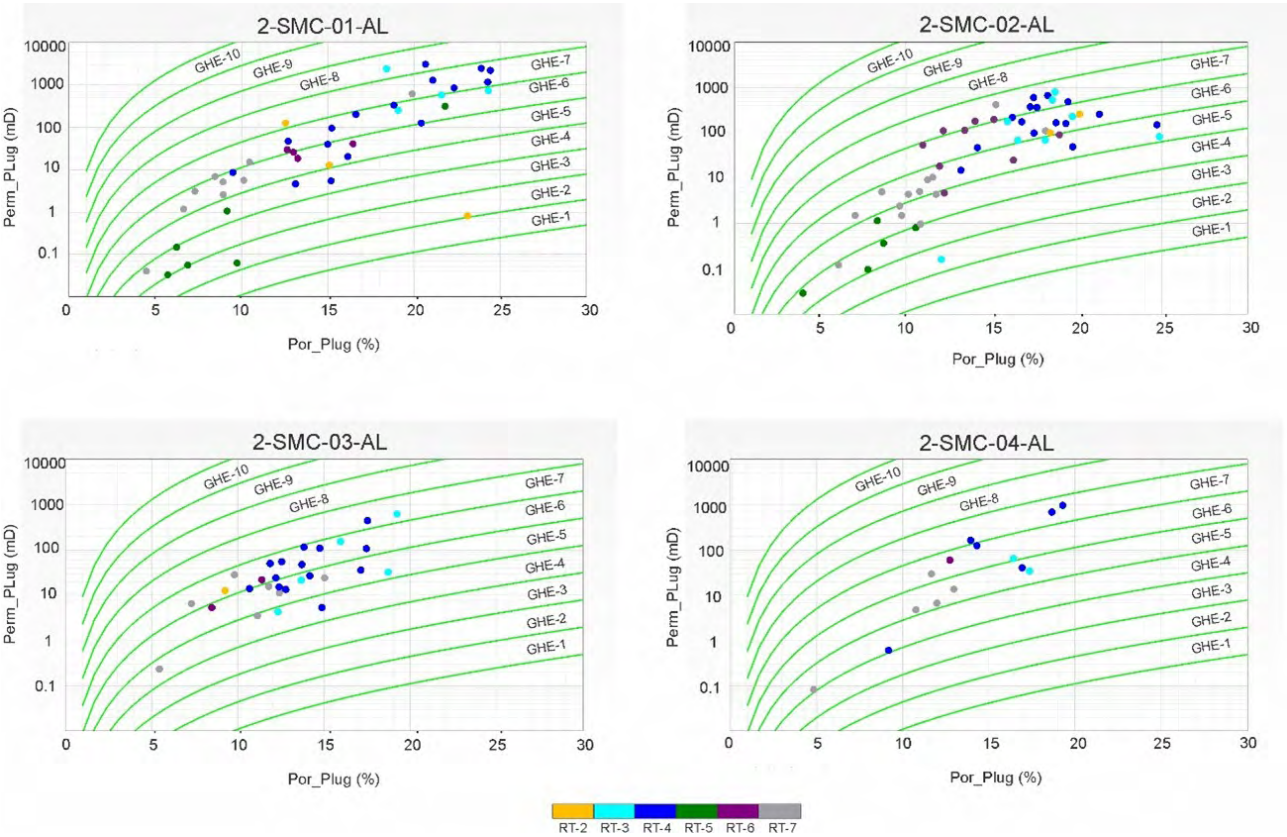
Figure 7 Classification of the Global Hydraulic Units (GHEs) of samples from the studied wells, based on porosity and permeability data.

of silty-clayey matrix lithologies and shows a depositional trend with less diagenetic influence. GHE-4 had mostly the presence of RT-7, which was composed of more cemented, compacted, and recrystallized lithologies; however, this element also had RT-4. This can be explained by the transitional lithologies in RT-7, placing some samples at cutoff limits between both Rock Types, besides compaction and moderate cementation nfluences.

In GHE-5, compacted, cemented, recrystallized pure coquinas were concentrated, with a homogeneous behavior of low porosity and permeability, which can be classified as a low-quality reservoir (Corbett et al. 2016). In GHE-6, RT-3 and RT-4 reflect petrophysical characteristics related to high-energy depositional environments, while in GHE-7 these Rock Types have higher permeabilities. This may have been influenced by diagenetic dissolution effects, which increase permeability to porosity ranges like those GHE-6 samples. GHE-8 contains Rock Types highly influenced by dissolution diagenesis only in the well 2-SMC-01-AL. This fact increases permeability and porosity ranges of the samples. Luna et al. (2016) attributed the presence of macropores in coquinas samples positioned in GHE-6, GHE-7, and GHE-8, as responsible for increases in permeability by dissolution of interparticle porosity and moldic porosity. This, in turn, increases porous media connectivity and can then evolve into vug porosity, classified as high-quality reservoir (Corbett et al. 2016). To evaluate the distribution of the intervals with the best and worst reservoir characteristics, the wells were correlated based on interpretations of Gamma Ray logs, Density, Rock Types, photoelectric factor, and porosity and permeability logs (Figure 8). Thus, two maximum flooding surfaces (MFS) correlated across the wells were interpreted, the lower MFS-P and upper MFS-C, which separate the Morro do Chaves Formation from Penedo and Coqueiro Seco Formations, respectively (Favoreto et al. 2021). To refine the correlation across the wells, three other internal surfaces were interpreted as flood surfaces (FS), two of which (FS-1L and FS-2L) in the lower section of the Morro do Chaves Formation. The FS-1L limits the top of a sequence of Rock Types interspersing clayey and hybrid matrix lithologies with silty-sandy matrix. These had more cemented and recrystallized intervals, corresponding to the sequences 1 and 2 by Favoreto et al. (2021). The FS-2L limits the top of a sequence of Rock Types with greater presence of cemented coquinas, stylolites due to compaction, and hybrid coquinas, which had greater presence of fracture, intercrystalline, and subordinate interparticle porosities, corresponding to the sequences 3 and 4 by Favoreto et al. (2021). Interpretations suggested a regressive surface (RS), dividing the Morro do Chaves Formation into two sections (upper and lower). The upper section was characterized by

Rock Types composed of coquinas with greater reworking of bivalve remains, which was interbedded with lithologies with greater amount of siliciclastic sandy material in the matrix, as well as predominance of interparticle, moldic, and vug porosities, which were interconnected and improved by dissolution, showing the highest porosity and permeability averages. The lower section was essentially composed of more compacted and cemented pure coquinas, with lower porosity and permeability averages. The petrophysical characteristics of both intervals were directly related to the lithologies described, as previously highlighted by other authors (Riguete et al. 2020; Favoreto et. al. 2021). The FS-1U surface, in the upper section of the Morro do Chaves Formation, limits the top of a sequence of Rock Types composed of lithologies with high concentrations of reworked bioclasts, as well as Rock Types composed of hybrid lithologies with higher proportions of sandy-clayey siliciclastic matrix, which were more frequent towards the top. The top of this sequence was limited by the MFS-C surface that separates the Morro from Chaves Formation from Coqueiro Seco Formation.

5 Conclusion

Seven Rock Types were interpreted in the Morro do Chaves Formation, one of muddy composition (RT-1), one of sandy matrix and reworked shells with dispersed composition (RT-2), two composed of shells well-sorted and reworked (RT-3 and RT-4), one of muddy matrix with dense packed shells (RT-5), and two of dense packed shells with compaction effects, being the last one with recrystallization (RT-6 and RT-7). The average porosity has a direct relationship with Rock Type lithologies, among which the most reworked ones had the highest porosity while the most clayey ones had the lowest, reflecting depositional control. Dissolutions related to diagenetic events increase porosity and permeability in lithologies with reworked shell fragments, which can occur associated to sandy siliciclastic matrix. On the other hand, porosity can be reduced when associated to compaction and recrystallization events, mainly related to pure coquinas with little presence of siliciclastic matrix. Six porosity types were identified, with three being selective (interparticle, moldic, and intercrystalline) and three nonselective (fracture, stylolite, and vug). Among the selective porosities, two (interparticle and moldic) were more frequent and represent the highest averages values, besides being mainly concentrated in the upper section of the studied wells, just as nonselective vug porosity. The nonselective porosities (intercrystalline, fracture, and stylolite) were more frequent in the lower section of the studied wells. The Dual-energy CT scan
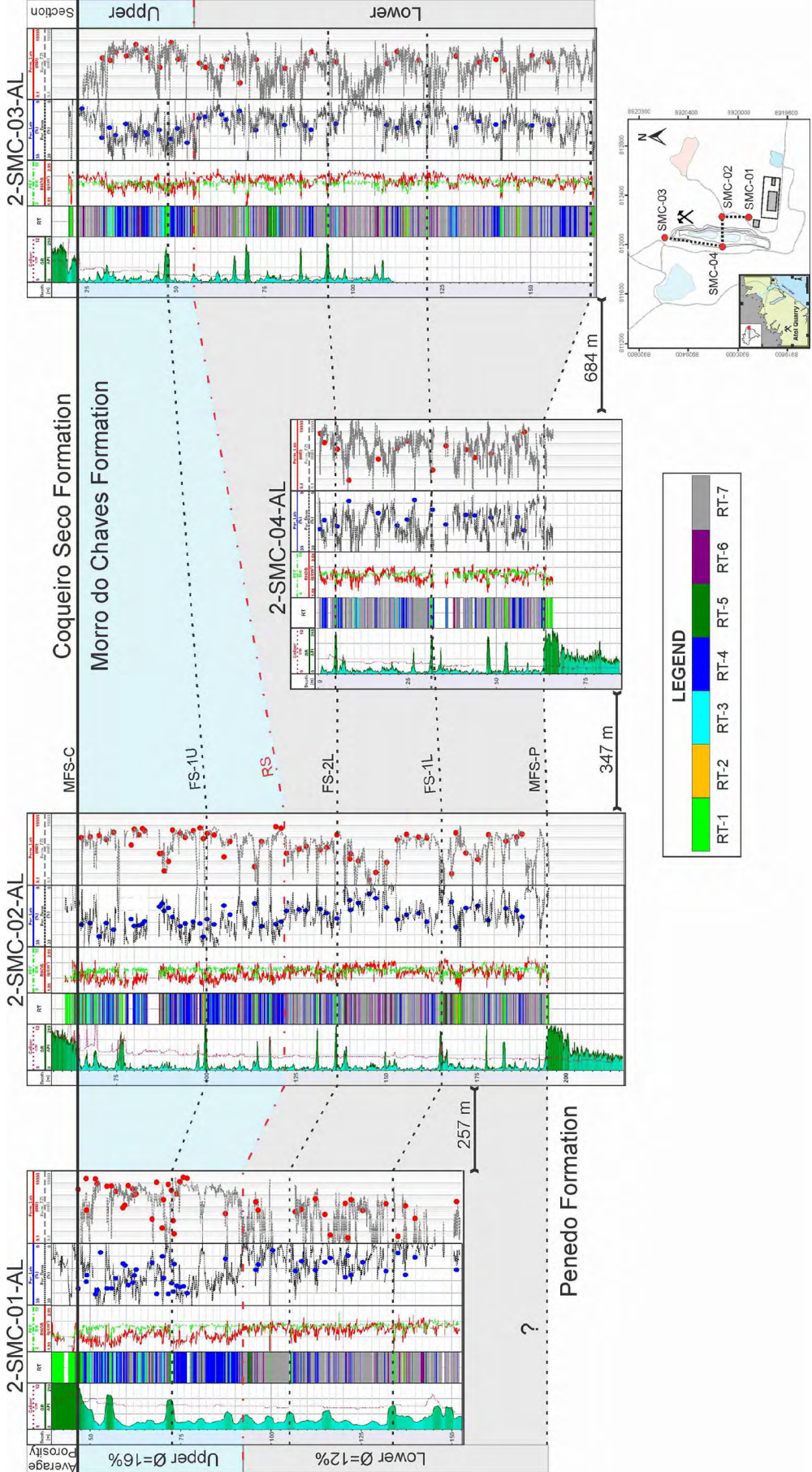
Petrophysical Characterization and Porosity-Permeability Log Calculation by Dual-Energy...

Mendes et al.

Figure 8 Stratigraphic correlation of the studied wells with the depth on the first track, Gama Ray (dark green) and Caliper (dark red) logs on the second track, Rock Types on the third track, Density (light red) and PEF (light green) logs on the fourth track, porosity log (black) with the plug porosities (blue dots) from laboratory on the fifth track and the permeability log (light gray) with the plug permeabilities (red dots) from laboratory on the sixfth track. The average porosity is 16% in the Upper zone and 12% in the Lower zone.

proved to be efficient in Rock Type characterization using RHOB and PEF logs, as well as for well porosity logs, showing high correlation with laboratory measurements on plugs. The Flow Zone Index (FZI) approach was effective in calculating well permeability logs, providing equations from regressions with high correlations with laboratory measurements of porosity and permeability. By correlating the wells drilled in the Atoll Quarry, two intervals with distinct petrophysical behaviors could be identified, which divide the Morro do Chaves Formation into upper and lower sections. The upper section presents the highest porosity and permeability averages due to depositional and diagenetic processes, which increased pore connectivity. This was also where the best reservoirs classified by the Global Hydraulic Elements (GHE) were found: GHE-6, GHE-7, and GHE-8. The lower section, in turn, presents the lowest porosity and permeability averages values, which was influenced by compaction and recrystallization diagenetic processes, which reduce pore flow capacity in poor reservoirs: GHE-2, GHE-3, GHE-4, and GHE-5.

6 Acknowledgments

7 References

Al-Owihan, H., Al-Wadi, M., Thakur, S., Behbehani, S., Al-Jabari, N., Dernaika, M. & Koronfol, S., 2014, 'Advanced rock characterization by dual energy CT imaging: a novel method in complex reservoir evaluation', *International Petroleum Technology Conference*, Doha, Qatar, viewed 20–22 January 2014, <https://onepetro.org/IPTCONF/proceedings-abstract/13IPTC/All-13IPTC/IPTC-17625-MS/153109>.

Amaefule, J.O., Altunbay, M., Tiab, D., Kersey, D.G. & Keelan, D.K. 1993, 'Enhanced reservoir description: using core and log data to identify Hydraulic (flow) units and predict permeability in uncored intervals/wells', *68th Annual Technical Conference and Exhibition*, Houston, TX, USA, viewed 3–6 October 1993, DOI:10.2118/26436-MS.

Azambuja, N.C., Arienti, L.M. & Cruz, F.E. 1998, 'Guidebook to the Rift-Drift Sergipe- Alagoas Passive Margin Basin'. *AAPG International Conference & Exhibition,* Brazil.

Cainelli, C. & Mohriak, W.U., 1999. 'Some remarks on the evolution of sedimentary basins along the Eastern Brazilian continental margin'. *Episodes 1999*, vol. 22, no. 3, pp. 206-16, DOI:10.18814/epiiugs/1999/v22i3/008.

Câmara, R.N. 2013. 'Caracterização petrofísica de coquinas da Formação Morro do Chaves (Barremiano/Aptiano), intervalo pré-sal da bacia de Sergipe-Alagoas', Dissertação de Mestrado, Universidade Federal do Rio de Janeiro, Rio de Janeiro.

Campos Neto, O.P.A., Souza-Lima, W. & Cruz, F.E.G. 2007. 'Bacia de Sergipe-Alagoas', *Boletim de Geociências da Petrobras*, vol. 15, pp. 405-15.

Chinelatto, G.F., Vidal, A.C. & Kuroda, M.C., 2018. 'A taphofacies model for coquina sedimentation in lakes (Lower Cretaceous, Morro do Chaves formation, NE Brazil)', *Cretaceous Research,* vol. 85, pp. 1–19, DOI:10.1016/j.cretres.2017.12.005.

Choquette, P.W. & Pray, L.C. 1970, 'Geologic nomenclature and classification of porosity in sedimentary carbonates', *AAPG (Am. Assoc. Pet. Geol.) Bull,* vol. 54, no. 2, pp. 207-50, DOI:10.1306/5D25C98B-16C1-11D7-8645000102C1865D.

Corbett, P.W.M. & Potter, D. 2004, 'Petrotyping: a basemap and atlas for navigating through permeability and porosity data for reservoir comparison and permeability prediction', *SCA Annual Conference*, Abu Dhabi, UAE.

Corbett, P.W.M., Estrella, R., Rodriguez, A.M., Shoeir, A., Borghi, L. & Tavares, A.C. 2016. 'Integration of cretaceous Morro do Chaves rock properties (NE Brazil) with the Holocene Hamelin Coquina architecture (Shark Bay, Western Australia) to model effective permeability', *Petroleum Geoscience,* vol. 22, no. 2, pp. 105-22, DOI:10.1144/petgeo2015-054.

Corbett, P.W.M., Wang, H., Câmara, R., Tavares, A.-C., Borghi, L., Perosi, F., Machado, A., Jiang, Z., Ma, J. & Bagueira, R. 2017. 'Using the Porosity Exponent (m) and Pore-Scale Resistivity Modelling to understand Pore Fabric Types in Coquinas (Barremian-Aptian) of the Morro do Chaves Formation, NE Brazil', *Marine and Petroleum Geology*, vol. 88, pp. 628–47, DOI:10.1016/j.marpetgeo.2017.08.032.

Dal' Bó, P.F., Favoreto, J., Valle, B., Mendes, M., Riguete, A. L., Borghi, L. & Porto-Barros, J.P. 2021, *Coquinas da Formação Morro do Chaves*, Editora Albatroz, Rio de Janeiro.

Favoreto, J., Valle, B., Borghi, L., Dal' Bó, P.F., Mendes, M., Arena, M., Santos, J., Santos, H., Ribeiro, C. & Coelho, P. 2021, 'Depositional controls on lacustrine coquinas from an early cretaceous rift lake: Morro do Chaves Formation, Northeast Brazil', *Marine and Petroleum Geology*, vol. 124, e104852, DOI:10.1016/j.marpetgeo.2020.104852.

Figueiredo, A.M.F. 1981. 'Depositional System in the Lower Cretaceous Morro Do Chaves and Coqueiro Seco Formations, and Their Relationship to Petroleum Accumulations, Middle Rift Sequence, Sergipe-Alagoas Basin', PhD Thesis, The University of Texas, Austin.

Kinoshita, E.M. 2010. 'Modelagem sísmica-geométrica de fácies dos carbonatos lacustres da Formação Morro do Chaves, Bacia de Sergipe-Alagoas', *Boletim de Geociências da Petrobras*, vol. 18, pp. 249–69.

Lima, M.C.O., Martins, L.P., Rios, E.H, Boyd, A., Pontedeiro, E.M.B.D., Hoerlle, F., Lipovetsky, T., Neto, A.O., Mendes, M., Borghi, L.F. & Couto, P. 2019, 'Rock typing of coquinas from the Morro do Chaves Formation', *16th International Congress of the Brazilian Geophysical Society*, Rio de Janeiro, Brasil, viewed 19-22 August 2019, < https://sbgf.org.br/

mysbgf/eventos/expanded_abstracts/16th_CISBGf/Rock%20 typing%20of%20coquinas%20from%20the%20Morro%20 do%20Chaves%20Formation.pdf>

Luna, J. L., Perosi, F.A., Ribeiro, M.G.S., Souza, A., Boyd, A., Borghi de Almeida, L.F. & Corbett, P.W.M. 2016. 'Petrophysical rock typing of coquinas from the Morro do Chaves Formation, Sergipe-Alagoas Basin (Northeast Brazil)', *Revista Brasileira de Geofísica*, vol. 34, no. 4, pp. 509–21, DOI:10.22564/rbgf.v34i4.883.

Nunes, M.A., Valle, B., Borghi, L., Favoreto, J. & Mendes, M. 2021, 'Multi-scale and multi-technique characterization of hybrid coquinas: A study case from the Morro do Chaves Formation (Barremian-Aptian of Sergipe-Alagoas Basin, Northeast Brazil)', *Journal of Petroleum Science and Engineering*, vol. 208, DOI:10.1016/j.petrol.2021.109718.

Rigueti, A.L., Dal' Bó, P.F., Borghi, L. & Mendes, M. 2020, 'Bioclastic accumulation in a lake rift basin: the early cretaceous coquinas of the Sergipe–Alagoas basin, Brazil', *Journal of Sedimentary Research*, vol. 90, no. 2, pp. 228–49, DOI:10.2110/jsr.2020.11.

Tavares, A.C., Borghi, L., Corbett, P., Nobre-Lopes, J. & Câmara, R. 2015, 'Facies and depositional environments for the coquinas of the Morro do Chaves Formation, Sergipe-Alagoas Basin, defined by taphonomic and compositional criteria', *Brazilian Journal of Geology*, vol. 45, no. 3, pp. 415-29, DOI:10.1590/2317-488920150030211.

Thompson, D.L., Stilwell, J.D. & Hall, M. 2015, 'Lacustrine carbonate reservoirs from early Cretaceous rift lakes of western Gondwana: pre-salt coquinas of Brazil and West Africa', *Gondwana Research*, vol. 28, no. 1, pp. 26–51, DOI:10.1016/j.gr.2014.12.005.

Weger, R.J. 2006, 'Quantitative pore/Rock Type parameters in carbonates and their relationship to velocity deviations', PhD Thesis, University of Miami, Coral Gables.

Wellington, S., & Vinegar, H., 1987. X-ray computerized tomography. Journal of Petroleum Technology, 39(08),885–898.https://doi.org/10.2118/16983-PA

Author contributions

Marcelo Mendes: conceptualization; formal analysis; methodology; validation; writing-original draft; writing – review and editing; visualization. **Julia Favoreto:** writing – review. **Marcos Nunes:** writing – review. **Ariely Riguete:** writing – review. **Bruno Valle:** writing – review. **Leonardo Borghi:** funding acquisition; supervision; review. **Patrick Corbett:** review. **Maira Lima:** editing. **Lorena Martins:** editing. **Michele Arena:** review.

Conflict of interest

The authors declare no potential conflict of interest.

Data availability statement

All data included in this study are publicly available in the literature.

Editor-in-chief

Dr. Claudine Dereczynski

Associate Editor

Dr. Joalice Mendonça

Como citar:

Mendes, M., Favoreto, J., Nunes, M., Rigueti, A., Valle, B., Borghi, L., Lima, M., Martins, L., Arena, M. & Corbett, P. 2023, 'Petrophysical Characterization and Porosity-Permeability Log Calculation by Dual-Energy CT Scan: Morro do Chaves Formation, Sergipe-Alagoas Basin, Brazil', *Anuário do Instituto de Geociências,* 46:47353. https://doi.org/10.11137/1982-3908_2023_46_47353